Approaches to Exploring Spatio-Temporal Surface Dynamics in Nanoparticles with *In Situ*Transmission Electron Microscopy

Ethan L. Lawrence¹, Barnaby D.A. Levin¹, Benjamin K. Miller²,

Peter A. Crozier^{1*}

¹School for the Engineering of Matter, Transport and Energy, Arizona State University, Tempe,
Arizona 85287, USA

²Gatan, Inc., Pleasanton, CA, USA.

*Corresponding author email: crozier@asu.edu

Abstract

Many nanoparticles in fields such as heterogeneous catalysis undergo surface structural fluctuations during chemical reactions, which may control functionality. These dynamic structural changes may be ideally investigated with time-resolved *in situ* electron microscopy. We have explored approaches for extracting quantitative information from large time-resolved image data sets with low signal-to-noise recorded with a direct electron detector on an aberration-corrected transmission electron microscope. We focus on quantitatively characterizing beam-induced dynamic structural rearrangements taking place on the surface of CeO₂ (ceria). A 2D Gaussian fitting procedure is employed to determine the position and occupancy of each atomic column in the nanoparticle with a temporal resolution of 2.5 ms and a spatial precision of 0.25 Å. Local rapid lattice expansions/contractions and atomic migration were revealed to occur on the (100) surface whereas (111) surfaces were relatively stable throughout the experiment. Application of this methodology to other materials will provide new insights into the behavior of nanoparticle surface reconstructions that were previously inaccessible using other methods, which would have important consequences for the understanding of dynamic structure-property relationships.

Keywords

in situ, structural dynamics, high temporal resolution, nanoparticle surfaces, AC-TEM, direct electron detector

1. Introduction

Recent developments in direct electron detectors for transmission electron microscopes has resulted in significant increases in image frame read-out speeds over conventional CCD imaging cameras, enabling temporal resolutions on the order of milliseconds to be achieved with high detective quantum efficiency (Faruqi et al., 2005; McMullan et al., 2014; Ruskin et al., 2013; Faruqi & McMullan, 2018). Installing these detectors on aberration-corrected transmission electron microscopes (AC-TEM) now allows materials characterization to be performed with both high spatial and temporal resolution. Structural dynamics are important in many areas of materials science and impact phase transformations, solid state reactions and morphological change. One area where this spatio-temporal analysis will be useful is for the study of atomic structural dynamics that may take place in catalytic nanoparticles under reaction conditions. *In situ* AC-TEM has become an indispensable tool for the direct observation of static and dynamic nanoparticle structures (Takeda et al., 2015; Takeda & Yoshida, 2013; Jinschek, 2014; Tao & Crozier, 2016; Taheri et al., 2016). Supported metal nanoparticles are extensively used in heterogeneous catalysis, and in situ atomic-level structural analysis can elucidate potential structure-reactivity relations (Helveg et al., 2004; Peng et al., 2012; Lawrence & Crozier, 2018). For many nanoparticle systems, particularly in catalysis, dynamic surface rearrangements can occur during a reaction and may be critical to functionality (Vendelbo et al., 2014; Kuwauchi et al., 2013; Yoshida et al., 2012). To achieve a fundamental understanding of atomic-level structural dynamics, it is therefore necessary to develop quantitative approaches for processing large series of noisy time-resolved images to extract structural information, such as the variation in atomic column positions and occupancies, with both high precision and the highest possible temporal resolution.

Methods have been developed to accurately determine atomic column positions or occupancies for atomic resolution images (Yankovich et al., 2014; Nilsson Pingel et al., 2018; Levin et al., 2016; Friedrich et al., 2009; Florea et al., 2013; Bals et al., 2016). However, to date these approaches have employed image averaging procedures or long acquisition times, which yields images with reasonable signal-to-noise. With the shorter acquisition times associated with improved temporal resolution, the signal-to-noise is significantly degraded, increasing the uncertainty associated with the determination of atomic column positions and occupancies. Another consequence of the high temporal resolution available from direct electron detectors is that extremely large data sets of a terabyte or more are generated, making it important to develop robust algorithms to automate extraction of meaningful information.

Here, we explore approaches for extracting quantitative information from large image data sets with low signal-to-noise recorded from nanoparticles undergoing dynamic surface structure rearrangement. For this work, we focus on CeO₂ (ceria) nanoparticles and use the electron beam to drive rapid structural reconfigurations at room temperature. Ceria is an important reducible metal oxide that has widespread technological applications due to its ability to exchange oxygen from its crystal lattice with the surrounding environment (Aneggi et al., 2016; Montini et al., 2016), and atomic-level structural heterogeneities can strongly influence the exchange activity (Trovarelli & Llorca, 2017; Tang & Gao, 2016). At elevated temperatures, especially under redox cycling, significant surface migration and sintering processes can take place (Crozier et al., 2008; Wang et al., 2010). Thus, developing time-resolved approaches to characterize atomic reconfigurations in ceria and other nanoparticle systems is critical to elucidate a fundamental mechanistic understanding of these processes. In this work, the electron beam accelerates the redox reactions at room temperature by preferentially removing oxygen, allowing us to acquire model data sets

that are ideal for developing the image processing techniques. Here, we achieve a spatial precision of 0.25 Å and single atom sensitivity for atomic column occupancies while the original temporal resolution of the image acquisition is preserved, revealing local lattice expansions and contractions on a ceria (100) surface that have not been previously observed in the literature. This approach does not only apply to beam-induced studies, rather, this work explores the capability of *in situ* TEM to observe structural dynamics regardless of how the structural changes are induced. The application of this methodology to other materials may provide new insights into the dynamic behavior of additional nanoparticle surfaces that were previously inaccessible using other methods, which can aid significantly in understanding structure-property relationships. For example, we have used the approach to explore oxygen vacancy creation and annihilation at different defect sites on oxide surfaces (Lawrence et al., 2018).

2. Materials and Methods

CeO₂ nanoparticles were synthesized by the hydrothermal method developed by Yang *et al.* (Yang et al., 2007, 2009). In a typical synthesis, Ce(NO₃)₃·6H₂O was dissolved into distilled water and mixed with a 12 M NaOH solution for 30 minutes with stirring. The resulting slurry was placed into a 50 mL autoclave and heated to 200°C for 24 hours. The precipitate was isolated by centrifugation, washed multiple times with de-ionized water, and dried at 60°C overnight in air to produce the desired CeO₂ nanoparticles.

An FEI Titan ETEM 80-300, aberration-corrected, environmental transmission electron microscope (AC-TEM) was used for imaging CeO₂ nanoparticles at 400 frames/second (fps). The microscope was operated at 300kV and used in ETEM mode with a pressure of <10⁻⁶ Torr at the

sample. (111) and (100) CeO₂ nanoparticle surfaces were imaged in a [110] projection at 120,000 e⁻Å⁻²s⁻¹, equating to 300 e⁻Å⁻² per individual frame. This electron fluence has been shown to induce dynamic structural rearrangements on ceria surfaces in vacuum at room temperature (Sinclair et al., 2017; Bhatta et al., 2012; Möbus et al., 2011; Bugnet et al., 2017). Images were acquired using a Gatan K2 IS direct electron detector operated at 400 fps with 4k x 4k pixels and a pixel size of ~0.125 Å/pixel. Images were acquired over a ~22 second total exposure time, equating to ~8800 individual image frames. Visual analysis of the full image sequence showed that structural rearrangements occurred throughout the observation period.

Representative dynamic events of ~500 ms (~200 image frames) were selected for image analysis. Initially, algorithms designed for use on annular dark field STEM images were applied to representative image sequences; however, these methods failed to give satisfactory results for our images. The bright and varying background of low signal-to-noise bright field TEM images makes it challenging to extract atomic column intensities and distinguish atomic columns from noise fluctuations, which motivated us to design our own more basic algorithm. To demonstrate our image analysis methodology, individual 2.5 ms exposure images were spatially binned by two (to ~0.25 Å/pixel) and then a 1-pixel radius Gaussian blur filter was applied to reduce noise using ImageJ. The mean and standard deviation (σ_{vac}) of the intensity in vacuum was measured, and these values were used to estimate the error due to noise as discussed below. All of the images were normalized by dividing each individual image by the mean vacuum intensity to set the vacuum level at 1. This facilitated comparison of experimental images with multislice simulations.

A suite of custom written MATLAB codes, which we named Time-Resolved Atomic Column Tracking (TRACT), was used to identify atomic columns and determine their position and integrated intensity (Levin et al., 2019). Analysis with the TRACT code was greatly simplified

when applied to images with bright atom contrast, rather than the dark contrast present in the initial images. Image contrast was therefore inverted by subtracting each pixel value from the mean These the **TRACT** codes available intensity in vacuum. are on Github (https://github.com/bdalevin/TRACT-TEM-Tracking-MATLAB-Code), and a brief description is given below. After loading image stacks into MATLAB, approximate positions for each cation column in the nanoparticle were identified manually. The position of each cation column in a summed image of the time series (a time-projected image) was then precisely located by first finding the local maximum within a user-specified radius from each initial position, fitting a centroid around each local maximum, and then fitting a 2D elliptical Gaussian around each centroid position. The coordinates of the maxima of each of the 2D Gaussians in the time-projected image defined the positions of each cation column. The centroid fitting stage of coding made use of the particle tracking scripts originally written for the programming language IDL by Crocker, Grier, and Weeks (Crocker & Grier, 1996), and implemented in MATLAB by Blair & Dufresne (Blair & Dufresne, 2011). The Gaussian fitting stage of coding made use of the 2D Gaussian MATLAB function written by Gero Nootz (Nootz, 2012).

Next, the cation column positions found in the time-projected image were used as initial estimates to determine the cation column positions in each individual frame of the image series. Due to the low signal-to-noise of the 2.5 ms exposure images, two additional criteria were applied to determine if each Gaussian fit in the individual frames was acceptable: the amplitude must be equal to or greater than $2\sigma_{vac}$ of the vacuum intensity value and the goodness of fit (R²) must be greater than 0.4. Assuming normal statistics, the probability of random noise causing the intensity to be greater than $2\sigma_{vac}$ of the vacuum intensity value is ~5%, and we therefore assume that this criterion provides 95% confidence that the Gaussian fit is associated with the presence of an atomic

column. *Supplementary Figure S1* provides a schematic of the requirement that a Gaussian fit must have an amplitude of greater than $2\sigma_{vac}$. If the amplitude of the Gaussian fit was less than $2\sigma_{vac}$, then the integrated intensity was set to zero. If the amplitude was equal or greater than $2\sigma_{vac}$ but the R² value was equal to or less than 0.4, then the fit was rejected and ignored during analysis. The coordinates of the maxima of each of the 2D Gaussians defined the positions of each cation column. A value for column intensity in each frame was calculated using the analytical expression for the integral of a 2D Gaussian function, $I = 2\pi A \sigma_x \sigma_y$, where A is the amplitude of the fit and σ_x and σ_y are the standard deviations (widths of the curves) of the two dimensions of the Gaussian function. The accuracy of the TRACT algorithm for locating atomic column positions and estimating column occupancy is critically discussed in (Levin et al., 2019).

AC-TEM image simulations were performed using a multislice approach in the JEMS software developed by Pierre Stadelmann to produce an image intensity look-up table (Stadelmann, 2018). For image simulations, the microscope accelerating voltage, spherical and chromatic aberration coefficients, beam half convergence angle, and defocus conditions were matched to experimental conditions while additional lens aberrations and noise were set to zero as shown in *Supplementary Table S1*. A partially coherent (envelope) illumination model was used. To calculate the intensity look-up table, images of a (111) CeO₂ surface were simulated over a range of thicknesses from 1 Ce atom per column to 16 Ce atoms per column corresponding to ~5 nm. A representative simulated image of 4-atom thickness is presented in *Supplementary Figure S2a*, and the corresponding inverted image used for intensity calculations is shown in *Supplementary Figure S2b*. A value for the intensity of Ce columns at each thickness was calculated by fitting a 2D elliptical Gaussian to columns at different sites using the procedure described above. Four different sites were chosen for intensity calculations: two sites at the (111)

surface of the simulated image, and two "bulk" sites several layers away from the (111) surface. 'A' sites are those where the Ce atoms in the column appear in the odd-numbered slices in our simulations and 'B' sites are those where the Ce atoms in the column appear in the even-numbered slices in our simulations. 'A' and 'B' sites were chosen to determine if there were any differences in intensity at different positions along the beam direction. The results of these calculations are given in the look-up table in *Supplementary Figure S2c*, which shows that the integrated intensity increases roughly linearly between 1 and 7 atoms in thickness, before peaking at 13 atoms in thickness and decreasing thereafter. Relatively little difference in integrated intensity is observed between different sites (A and B, surface and bulk) until 10 atoms in thickness is reached.

3. Results and Discussion

3.1. Imaging Surface Structures

Figure 1a shows an AC-TEM image of a ~2 nm CeO₂ nanoparticle with a 1 s total exposure time (unprocessed 2.5 ms frames aligned and summed together). Cerium atomic columns have dark contrast in these images; oxygen atomic columns were not visible with the imaging conditions used. Figure 1b shows a single, unprocessed 2.5 ms exposure frame from the image sequence used to create the 1 s total exposure image in Figure 1a, indicating the low signal-to-noise ratio present in individual images. As evidenced by Figure 1a,b, higher temporal resolution is associated with lower signal-to-noise in the raw data. In this orientation, a polar (100) facet is flanked by two non-polar (111) facets. Inspection of the nanoparticle surfaces in Figure 1a reveals that the atomic columns on the (100) surface appear more diffuse relative to the (111) surfaces and subsurface atomic columns. Variation in the positions and intensities of atomic columns in individual frames

causes the more diffuse appearance of columns on the (100) surface, and it is these variations that we aim to characterize.

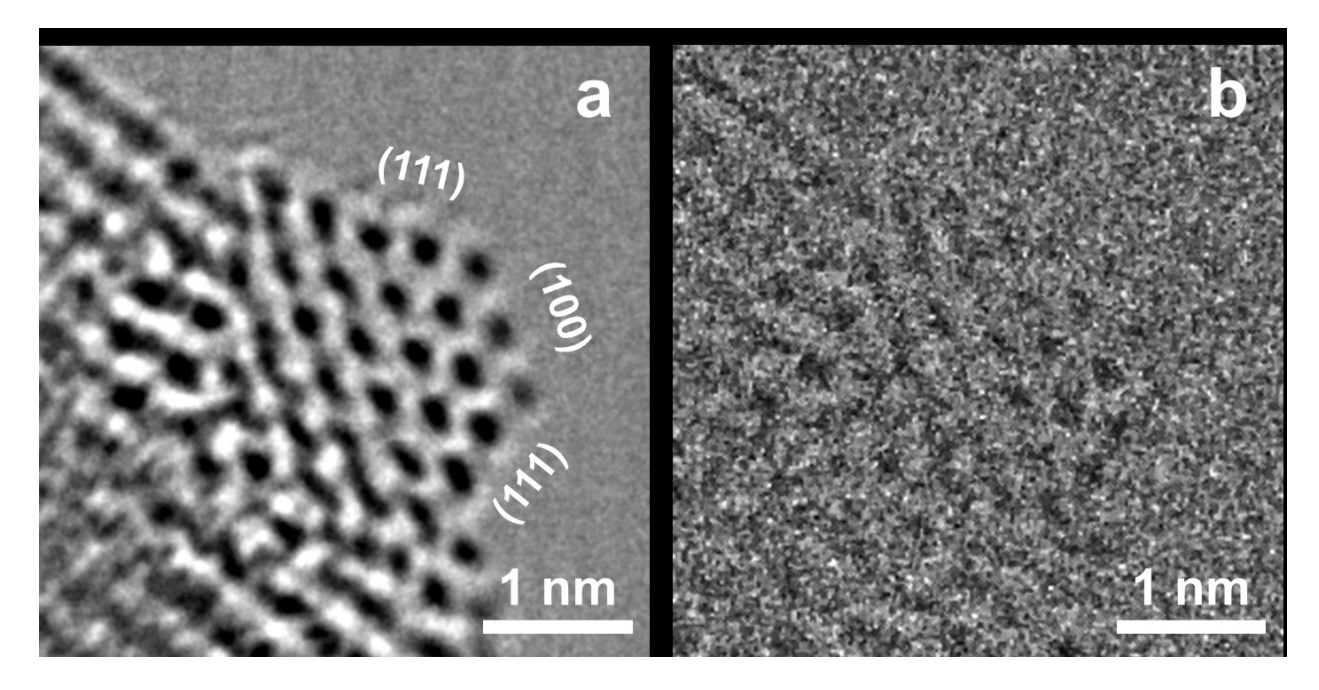


Figure 1. Imaging of a CeO₂ nanoparticle. **a** Aberration-corrected TEM image of a ~2 nm CeO₂ nanoparticle with a 1 s total exposure time (unprocessed 2.5 ms frames aligned and summed together). **b** A single, unprocessed 2.5 ms exposure frame from the image sequence used to create the 1 s total exposure image in **a**.

3.2. Relationship between Measurement Precision and Temporal Resolution

It is important to consider the relationship between the precision of position/intensity measurements and the temporal resolution. Consider an atomic column that is assumed to be stationary and does not change occupancy throughout the observation period. If Poisson statistics is assumed and M independent measurements of position, r, or intensity, I, are made, then the average of those M measurements provides the best estimate of the "true" value with the standard error in the mean given by σ_M/\sqrt{M} where σ_M is the standard deviation. For an individual

measurement from a single frame, the standard deviation, σ_M , provides an estimate of the uncertainty/error associated with each individual measurement.

For atomic column position analysis, columns in the center of the nanoparticle image composed mainly of subsurface atoms are more stationary than surface columns over the representative observation period (200 image frames) and can be used to estimate the standard deviation associated with the precision of the measurement technique. The standard deviation of the position of those columns was ~ 0.25 Å. We assumed the measurement error, σ_0 , of the more dynamic surface columns was also 0.25 Å for each 2.5 ms exposure frame. The temporal resolution limit is defined as t_0 with $t_0 = 2.5$ ms for these experiments. Thus, σ_0 represents the spatial precision in the determination of the position of an atomic column with a temporal resolution of t₀. If n frames are averaged together, the temporal resolution is degraded to $t_n = nt_0$, but the spatial precision of the average position measurement would improve to $\sigma_n = \sigma_0/\sqrt{n}$. Solving for n = t_n/t_0 and inserting into σ_n gives $\sigma_n = \sigma_0 \sqrt{\frac{t_0}{t_n}}$, which provides a simple expression relating the spatial precision to the temporal resolution. It shows that for a given electron fluence per frame, there is an inverse relationship between spatial precision and temporal resolution. This relationship is plotted in Figure 2 (including the electron fluence) for the experimental parameters described above. As can be seen from this plot, the spatial precision is 0.25 Å at the limiting case of 2.5 ms temporal resolution but can be improved by averaging images together. For example, if 0.05 Å spatial precision is desired, then the temporal resolution must be reduced to 62.5 ms, which corresponds to 25 frames being averaged together. It is interesting to note that the curve initially falls rapidly with temporal resolution and averaging 5 frames (12.5 ms) gives over a factor of 2 improvement in spatial precision. However, to achieve another factor of 2 would require averaging

of 25 frames because the curve drops more slowly. Similarly, reducing the fluence by a factor of 5 would degrade the spatial precision only by a factor of 2.

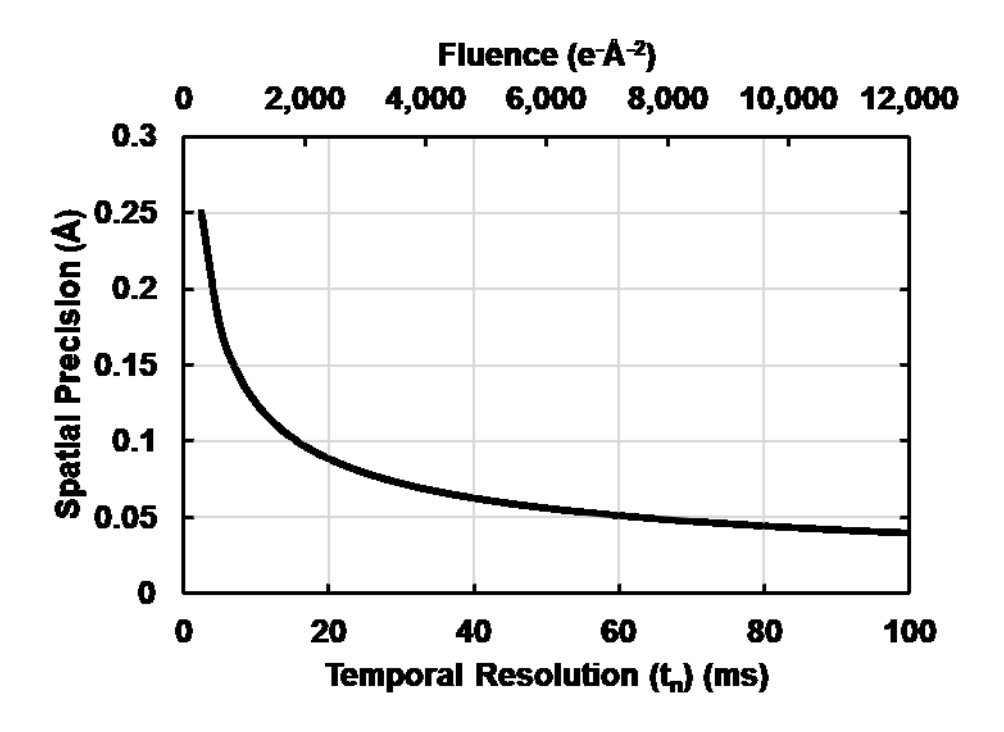


Figure 2. Relationship between spatial precision, temporal resolution, and electron fluence.

Similarly, for intensity analysis, atomic columns in the center of the nanoparticle image visually appeared to have relatively constant intensity over the representative observation period (200 image frames), and the standard deviation of the integrated intensity of those columns was measured to be ~0.3 arbitrary units. Therefore, the precision of individual measurements of intensity is defined as $\Delta I_0 = 0.3$ arbitrary units at the temporal resolution limit of $t_0 = 2.5$ ms. Using the same arguments as discussed above for position measurements, if n image frames are averaged together and temporal resolution is sacrificed, then the precision of the average intensity measurement would be given by $\Delta I_n = \Delta I_0/\sqrt{n}$. This results in a similar expression for relating the intensity precision and temporal resolution of a single image frame to any number of averaged

images, $\Delta I_n \sqrt{t_n} = \Delta I_0 \sqrt{t_0}$. Therefore, the relationship between average intensity measurement precision and temporal resolution displays identical behavior to that shown for spatial precision in *Figure 2*.

3.3. Observing Local Surface Lattice Expansion & Contraction

Local lattice expansions and contractions were observed on the (100) surface over short time periods (~0.2 s), and the position of each Ce atomic column in the nanoparticle in each 2.5 ms image frame was determined. *Figure 3* shows a 0.5 s time sequence from the experiment during which a representative lattice expansion and contraction event was observed. The individual column positional measurement errors of 0.25 Å were added in quadrature to assign error bars of 0.35 Å to separation distance measurements in 2.5 ms image frames. For visual clarity, each image in *Figure 3* is a 12.5 ms exposure image (five spatially binned and Gaussian blurred 2.5 ms images summed together), which resulted in the error in separation distance to be reduced to 0.16 Å for these frames (0.35 Å/ $\sqrt{5}$). Images of *Figure 3* are shown with dark atom contrast, but the measurement analysis was performed on the inverted images. The separation distance between Ce atomic columns on the bulk-terminated (100) surface is 3.825 Å in this projection. As shown in Figure 3a, the distance between two (100) surface Ce atomic columns is 3.27±0.16 Å at 0.16 s, expands to 5.03±0.16 Å after 0.21 s (Figure 3b), and contracts back to 3.52±0.16 Å after an additional 0.2 s (*Figure 3c*). In *Figure 3a*, there are three (100) surface atomic columns; however, the third surface atomic column is almost invisible in *Figure 3b* when the lattice expansion occurs.

A time-resolved image sequence of the lattice expansion and contraction seen in *Figure* 3a-c is provided as *Supplementary Video V1*. The separation distance between the two (100) surface Ce atomic columns highlighted in *Figures 3a-c* was determined for each 2.5 ms frame in

the 0.5 s image sequence (200 frames) and is shown in *Figure 3d*. The blue points indicate measurements from each individual frame, the solid black line is a 5-frame moving average trendline, and the dashed green line indicates the bulk-terminated (100) separation distance (3.825 Å). The semi-transparent blue windows represent the five image frames that were summed together to create *Figures 3a-c*. The local lattice expansion and contraction behavior was cyclical and occurred several times over the full set of experimental image acquisitions (~22 s) (An additional sequence and quantification is shown in *Supplementary Figure S3*).

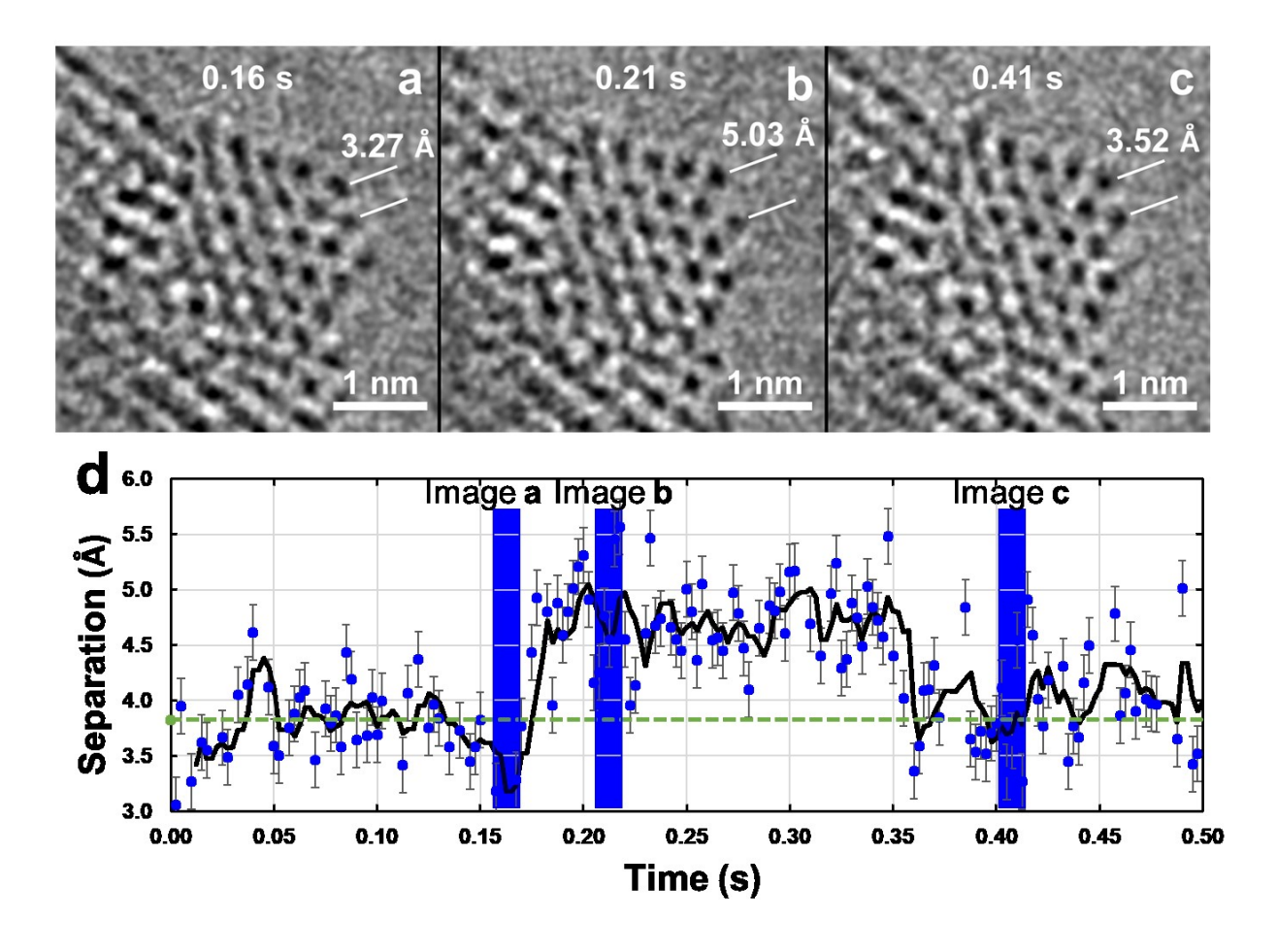


Figure 3. Local surface lattice expansion. **a-c** Image sequence of the CeO₂ nanoparticle with 12.5 ms exposure images (five spatially binned and Gaussian blurred 2.5 ms images summed together). Two Ce atomic columns on the (100) surface are separated by 3.27 Å at 0.16 s in **a**, expand to 5.03 Å after 0.21 s in **b**, and contract to 3.52 Å after 0.41 s in **c**. **d** Measurement of the separation of the

two marked surface Ce atomic column over 0.5 s image sequence. The blue points indicate measurements from each frame, the solid black line is a 5-frame moving average trendline, and the dashed green line indicates the bulk-terminated (100) separation distance (3.825 Å). Error bars are 0.35 Å. The semitransparent blue windows represent the five image frames that were summed together to create **a-c**.

As can be seen in *Figure 3d*, the drastic expansion of the atomic column separation occurs over a short time period. This expansion is shown in *Figure 4* with 2.5 ms temporal resolution. In Figure 4a,e, the distance between the two (100) surface atomic columns is 3.77±0.35 Å. After 2.5 ms, the three surface atomic columns are absent from the image (Figure 4b,f). The absence of visible contrast for the three surface atoms in Figure 4b,f may indicate that the atoms are dynamically rearranging, causing diffuse image signal that is indiscernible from the noise. Alternatively, if it's assumed that an atomic column is present and stationary, then based on the criteria described in Materials and Methods, for the column to be visible it must have an intensity value of $I > I_{vac} + 2\sigma_{vac}$. If the intensity is less than $I_{vac} + 2\sigma_{vac}$, the column will be undetectable. As a result, it can be inferred that the absence of visible signal for the three surface atomic columns in *Figure 4b,f* is either because the atoms are in a 'transition state' where atoms are dynamically rearranging during the exposure time or the atoms are stationary and have signal that is below the detection limit. It seems unlikely that three adjacent, stationary atomic columns would be invisible in the same 2.5 ms frame, so it is much more likely that the three columns are undergoing dynamic rearrangement. In the following frame (*Figure 4c,g*), the signal from the surface atomic columns is visible again, with the separation distance between the two atomic columns increasing to 4.43±0.35 Å. After an additional 2.5 ms, the expansion reaches 4.93±0.35 Å, as shown in *Figure*

4d,h. Although the individual image frames of *Figure 4* are quite noisy, this approach can clearly extract information about the precise time over which the surface lattice expansion took place.

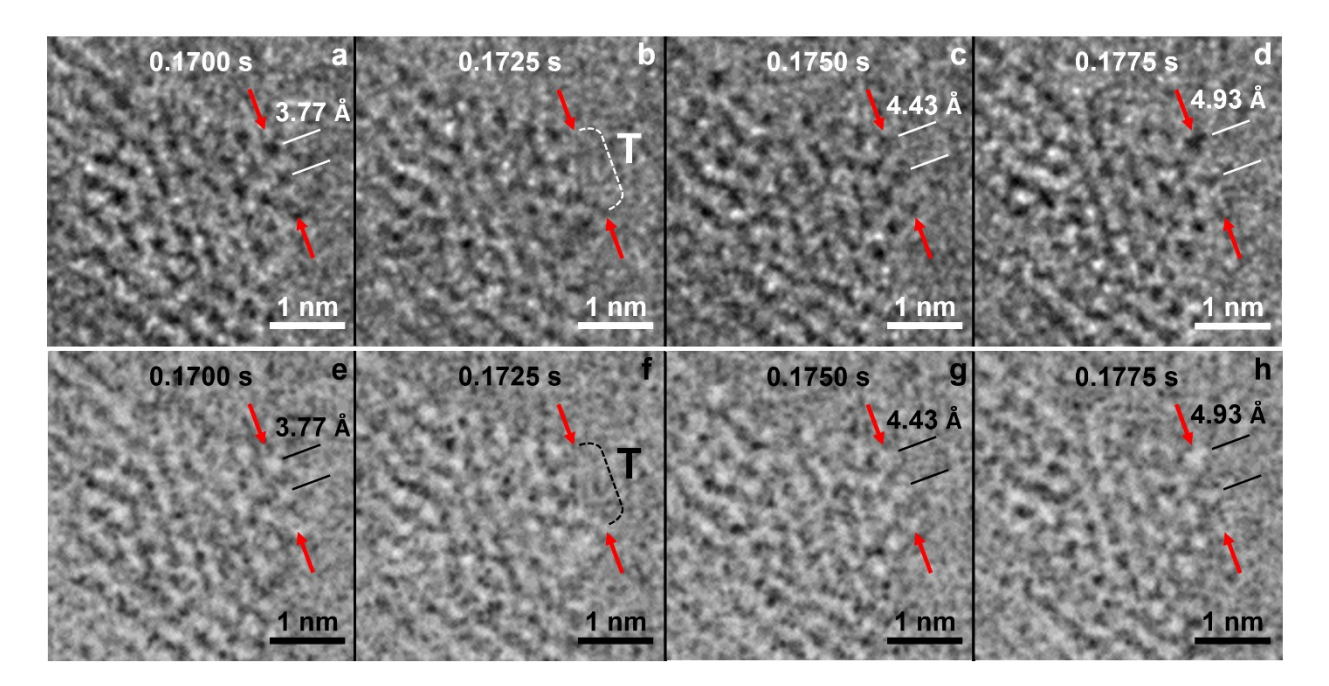


Figure 4. Image sequence of local (100) surface lattice expansion of CeO₂ nanoparticle with spatially binned and Gaussian blurred 2.5 ms frames in **a-d** and inverted images in **e-h**. Two surface atomic columns are separated by 3.77 Å in **a,e**, are absent in **b,f**, reappear and expand to 4.43 Å in **c,g**, and expand further to 4.93 Å in **d,h**. The error in each of these measurements is ±0.35 Å. The absence of the three (100) surface atomic columns in **b,f** suggests that the atoms in these columns are dynamically rearranging in a 'transition state', as marked by the "T" on the images. The red arrows in each frame provide a guide to the eye for referencing the surface dynamics.

This large and rapid local surface lattice expansion and contraction behavior on a CeO₂ nanoparticle (100) surface has not previously been reported in the literature and has been observed here for the first time due to the high temporal resolution of these measurements. It is hypothesized

that this behavior is related to a cyclic oxygen vacancy creation and annihilation process possibly driven in part by the electron beam and oxygen species (i.e. H₂O, O₂, OH* etc...) present in the environmental sample cell and possible oxygen migration from the bulk. The large expansion of the Ce spacing is likely associated with removal of the shared O anions, leading to strong electrostatic repulsion between the cations. This expansion may also have destabilized the third atomic column in *Figure 3* and caused the atoms in that column to migrate to more stable positions. In addition, (100) CeO₂ surfaces are known to more readily release oxygen compared to (111) surfaces due in part to their lower oxygen vacancy formation energy (Nolan et al., 2006; Paier et al., 2013; Skorodumova et al., 2002; Migani et al., 2010). Since we are removing oxygen with the electron beam, the cross section for removing oxygen via sputtering or knock-on will be larger on the (100) surface compared to the (111) surface. The lower vacancy formation energy may explain why more dynamic behavior is observed on (100) surfaces in our experiment and other studies (Bugnet et al., 2017; Sinclair et al., 2017; Möbus et al., 2011; Bhatta et al., 2012). These hypotheses can be confirmed with future theoretical simulations.

3.4. Observing Atom Migration

The integrated intensity of each Ce atomic column in each 2.5 ms image frame was quantified to estimate the number of atoms within each atomic column during surface migration. *Figure 5* shows a representative atom migration sequence of events during 0.5 s of the experiment, and each image is a 12.5 ms exposure of the inverted images used for analysis (five inverted 2.5 ms images summed together). Focusing on the three atomic columns identified by the white arrows and the "1", "2", and "3" labels (referred to as atomic column 1, atomic column 2, and atomic column 3, respectively), it is shown in *Figure 5a* that an atomically sharp tip has formed on the nanoparticle as indicated by the presence of atomic column 1 and absence of atomic column 2.

After 0.21 s (*Figure 5b*), every atom has migrated out of atomic column 1 as evidenced by the lack of intensity, whereas atoms have appeared in atomic column 2. Within an additional 0.11 s, some atoms have migrated back into atomic column 1 (*Figure 5c*). A time-resolved image sequence of the atom migration events seen in *Figure 5a-c* is provided as *Supplementary Video V2* and is also highlighted with 0.1 s exposure images in *Supplementary Figure S4*.

The number of Ce atoms within atomic columns 1, 2, and 3 were estimated through a comparison of experimental column intensities to the intensity look-up table (Supplementary Figure S2) and is shown in Figure 5d,e,f, respectively. The points indicate atomic column occupancy measurements from each 2.5 ms frame, the solid black line is a 5-frame moving average trendline, and the semitransparent red windows represent the five image frames that were summed together to create *Figures 5a-c*. As discussed in Materials and Methods, the standard deviation of the integrated intensity measurements of subsurface atomic columns in the center of the nanoparticle was ~0.3 arbitrary units, which is approximately the intensity value for a single atom as shown in Supplementary Figure S2. Therefore, error bars of ± 1 atom were assigned to the atomic column occupancy estimates of *Figure 5*. This error is relatively large but would be reduced if a higher electron flux is used or by sacrificing temporal resolution and averaging images together, both of which would increase the signal-to-noise and improve the Gaussian fitting procedure. The integrated intensity was set to 0 when an atomic column was unable to be fitted with a 2D Gaussian according to the criteria described in Materials and Methods, which could mean that no atoms are in that position, the atoms are dynamically rearranging and causing weak signal, or the signal-to-noise was too low to accurately determine a Gaussian fit.

As shown by the black trendline in *Figure 5d*, atomic column 1 has \sim 2-4 atoms until a sharp drop around 0.17 s, indicating that atoms are migrating out of the column. Additionally, in

Figure 5e, it is shown that atomic column 2 is absent until ~0.12 s and jumps up to ~2-3 atoms around 0.17 s, indicating the migration of atoms into the column. In Figure 5f, the occupancy of atomic column 3 is consistently ~3-5 atoms throughout the 0.5 s image sequence. Although noise causes some of the fluctuations observed in these three atomic columns, the main source of fluctuation is the change in occupancy, suggesting that atoms are continuously migrating during the observation period. For example, in Figure 5d there are two frames (red data points) around ~0.4 s where the estimated number of atoms are much higher than the surrounding data points. This image sequence is provided in Supplementary Figure S5 and confirms that the large increase in the estimated number of atoms is caused by atoms migrating into and out of atomic column 1 over a short time period. Furthermore, the appearance of the atomic columns depends on the selection of individual image frames that are summed together to make the shown frame. For instance, if the 200 individual images of the 0.5 s image sequence of Figure 5 were summed together into a single 0.5 s exposure image, atomic columns "1" and "2" would appear diffuse due to their absence/mobility in the individual image frames.

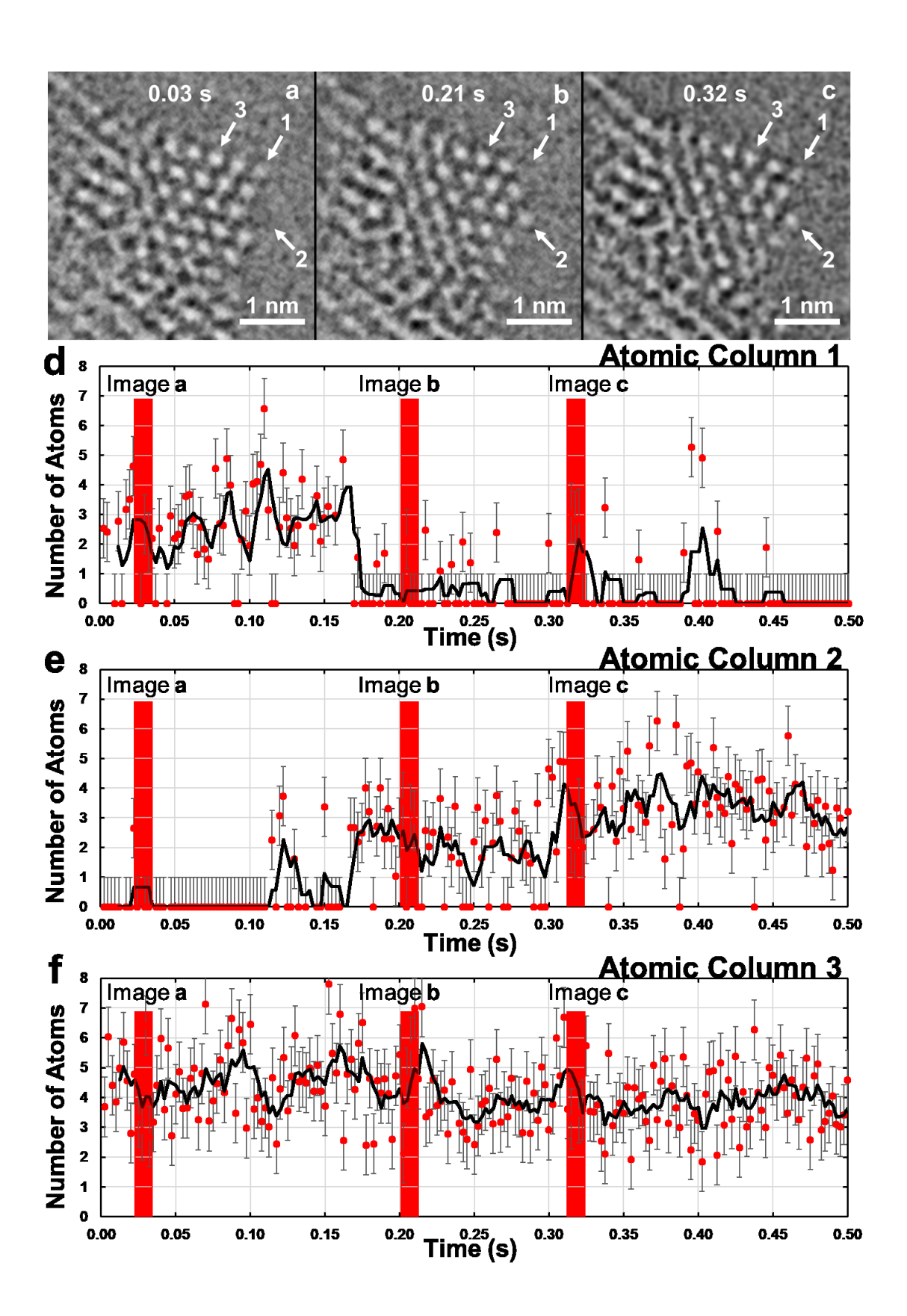


Figure 5. Atom migration. **a-c** Image sequence of the CeO_2 nanoparticle with 12.5 ms exposure images of the inverted images used for MATLAB analysis (five inverted 2.5 ms images summed together). As indicated by the "1", "2", and "3" labels, atoms are migrating into and out of these atomic columns during the observation period. **d,e,f** Estimated atomic column occupancy based on measurements of the integrated intensity from atomic column "1", "2", and "3", respectively, over a 0.5 s image sequence. The points indicate measurements from each frame and the solid black line is a 5-frame moving average trendline. The semitransparent red windows represent the five image frames that were summed together to create **a-c**. Error bars are ± 1 atom.

To construct a pseudo-3D representation of the nanoparticle, the number of Ce atoms within each atomic column was estimated. A wedge profile model at the (100) surface was assumed based on the truncated octahedral or tetrahedral CeO2 nanoparticle models observed in other studies (Wang & Feng, 2003; Migani et al., 2012; Tan et al., 2011; Sayle et al., 2004). Approximating the number of atoms in each column in individual frames can therefore observe the evolution of the pseudo-3D structure of the nanoparticle over time. The experimental occupancy estimations of individual frames fluctuate dramatically in *Figure 5d,e,f*, so the 5-frame moving average values were used to estimate the number of Ce atoms in each atomic column, which reduced the error to ~±0.5 atom. The relationship between electron fluence, temporal resolution and intensity measurement is important for the design of *in situ* experiments to explore structural dynamics. The authors give a detailed discussion of the accuracy of intensity measurements as a function of electron fluence per frame in (Levin et al., 2019). For each image in *Figure 5a-c*, a simple 3D model is shown in *Figure 6* where blue spheres represent Ce atoms and each atomic column has ~0-5 atoms. As was also evidenced in *Figure 5*, Ce atoms migrated out of atomic column 1 as atoms appeared in atomic column 2. Oxygen atomic columns are omitted

as they are not visible in our images and no conclusions can be drawn about their occupancy. Noise fluctuations may influence the atom counting procedure; however, our time-resolved pseudo-3D approach can still provide informative results such as visualization of 3D surface heterogeneity, preferential migration of atoms along a specific direction, or instabilities of a certain surface facet. For more precise quantification of atomic column occupancy, temporal resolution can be sacrificed to sum together more individual image frames for a higher signal-to-noise ratio. Although beyond the scope of the present manuscript, the pseudo-3D representation of this CeO₂ nanoparticle may be used to guide future theoretical studies as it gives a near real-time look into actual structures that are dynamically reconstructing on polar and non-polar surfaces. A time-resolved model representation provides the ability to detect subtle changes in surface morphology during *in situ* chemical reactions, which can then be compared to theoretically derived structural models to identify and confirm catalytically active sites, metastable phases, and other scientifically valuable information.

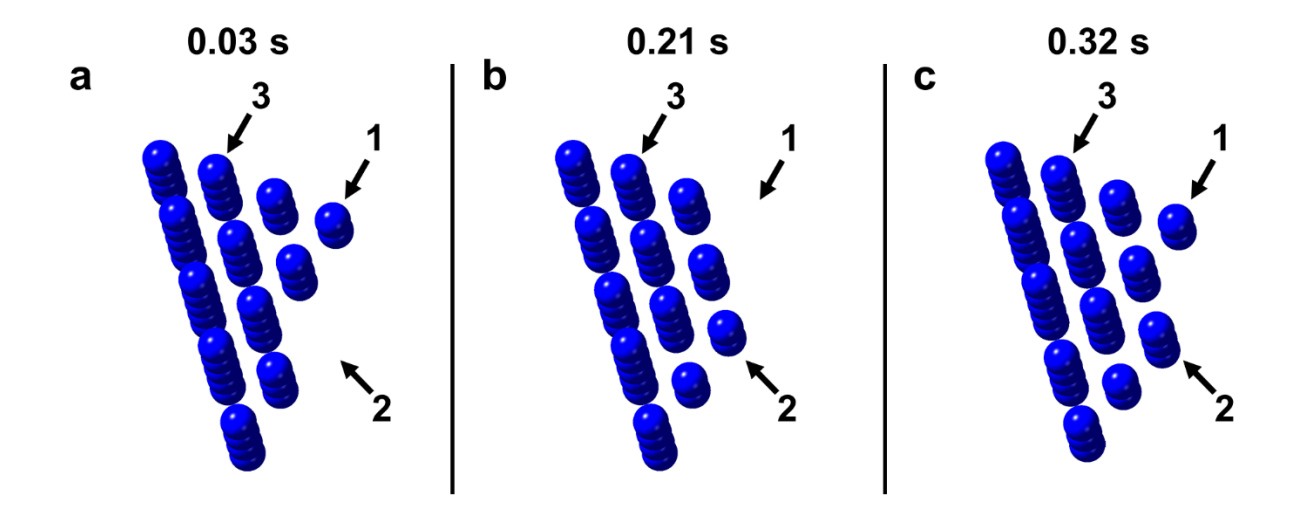


Figure 6. Simple 3D model showing number of atoms estimated in each column of the CeO₂ nanoparticle from the images of Figure 4a-c. Blue spheres represent Ce atoms. Oxygen atomic

columns are omitted because they are not visible in our images and no conclusions can be drawn about their occupancy. Error is estimated to be a max of ~±0.5 atom/column.

4. Conclusions

We have explored approaches for extracting quantitative information from large image data sets with low signal-to-noise recorded from nanoparticles undergoing dynamic surface structure rearrangement. For this work, we focus on CeO₂ (ceria) nanoparticles and experiments were performed on an AC TEM equipped with a direct electron detector running at 400 frames per second. We observed dynamic nanoparticle surface structures with 0.25 Å spatial precision and 2.5 ms temporal resolution. For fixed electron flux, improved spatial precision can only be achieved by degrading the temporal resolution. The position and occupancy of each atomic column within a CeO₂ nanoparticle was determined using a 2D Gaussian fitting and image simulation procedure. Due to the high spatial precision and temporal resolution, local rapid lattice expansions/contractions and atomic migration were revealed to occur on the (100) surface whereas (111) surfaces were stable throughout the experiment. A pseudo-3D representation was constructed by estimating each atomic column's occupancy, enabling the visualization of the dynamic evolution of the surface structure. This work provides a time-resolved approach for atomic-level in situ imaging of dynamic surface structures and can be applied to other nanomaterials systems to accelerate understanding of dynamic structure-property relationships.

Acknowledgements

We gratefully acknowledge NSF DMR-1308085 for support and Arizona State University's John M. Cowley Center for High Resolution Electron Microscopy for microscope use. We thank Gatan, Inc. for the loan and installation of a K2 IS direct electron detection camera.

Supplementary Information

Video V1. Video of lattice expansion and contraction (frames 4600-4800)

Video V2. Video of atom migration (frames 3150-3350)

Figure S1. Gaussian fitting criteria diagram.

Table S1. Image simulation parameters.

Figure S2. Simulated images and look-up table of simulated integrated intensity vs number of Ce atoms.

Figure S3. Additional image sequence and quantification of local surface lattice expansion and contraction.

Figure S4. 0.1 s exposure images of atomic migration event seen in Figure 5.

Figure S5. Fluctuation in atomic column occupancy.

References

- ANEGGI, E., BOARO, M., COLUSSI, S., DE LEITENBURG, C. & TROVARELLI, A. (2016). Chapter 289 Ceria-Based Materials in Catalysis: Historical Perspective and Future Trends. In *Handbook on the Physics and Chemistry of Rare Earths*vol. 50, Bünzli, J.-C. G. & Pecharsky, V. K. (Eds.), pp. 209–242. Elsevier http://linkinghub.elsevier.com/retrieve/pii/S0168127316300046 (Accessed October 25, 2017).
- BALS, S., GORIS, B., DE BACKER, A., VAN AERT, S. & VAN TENDELOO, G. (2016). Atomic resolution electron tomography. *MRS Bulletin* 41, 525–530.
- BHATTA, U. M., ROSS, I. M., SAYLE, T. X. T., SAYLE, D. C., PARKER, S. C., REID, D., SEAL, S., KUMAR, A. & MÖBUS, G. (2012). Cationic Surface Reconstructions on Cerium Oxide Nanocrystals: An Aberration-Corrected HRTEM Study. *ACS Nano* 6, 421–430.
- BLAIR, D. & DUFRESNE, E. (2011). *The Matlab Particle Tracking Code Repository*. http://physics.georgetown.edu/matlab/.
- BUGNET, M., OVERBURY, S. H., WU, Z. & EPICIER, T. (2017). Direct visualization and control of atomic mobility at {100} surfaces of ceria in the environmental transmission electron microscope. *Nano Letters*. http://pubs.acs.org/doi/10.1021/acs.nanolett.7b03680 (Accessed November 26, 2017).
- CROCKER, J. C. & GRIER, D. G. (1996). Methods of digital video microscopy for colloidal studies. *Journal of colloid and interface science* **179**, 298–310.
- CROZIER, P. A., WANG, R. & SHARMA, R. (2008). *In situ* environmental TEM studies of dynamic changes in cerium-based oxides nanoparticles during redox processes. *Ultramicroscopy* **108**, 1432–1440.
- FLOREA, I., FERAL-MARTIN, C., MAJIMEL, J., IHIAWAKRIM, D., HIRLIMANN, C. & ERSEN, O. (2013). Three-Dimensional Tomographic Analyses of CeO₂ Nanoparticles. *Crystal Growth & Design* **13**, 1110–1121.
- FRIEDRICH, H., DE JONGH, P. E., VERKLEIJ, A. J. & DE JONG, K. P. (2009). Electron Tomography for Heterogeneous Catalysts and Related Nanostructured Materials. *Chemical Reviews* **109**, 1613–1629.
- HELVEG, S., LÓPEZ-CARTES, C., SEHESTED, J., HANSEN, P. L., CLAUSEN, B. S., ROSTRUP-NIELSEN, J. R., ABILD-PEDERSEN, F. & NØRSKOV, J. K. (2004). Atomic-scale imaging of carbon nanofibre growth. *Nature* **427**, 426–429.
- JINSCHEK, J. R. (2014). Advances in the environmental transmission electron microscope (ETEM) for nanoscale *In situ* studies of gas—solid interactions. *Chemical Communications* **50**, 2696.

- KUWAUCHI, Y., TAKEDA, S., YOSHIDA, H., SUN, K., HARUTA, M. & KOHNO, H. (2013). Stepwise Displacement of Catalytically Active Gold Nanoparticles on Cerium Oxide. *Nano Letters* **13**, 3073–3077.
- LAWRENCE, E. L. & CROZIER, P. A. (2018). Oxygen Transfer at Metal-Reducible Oxide Nanocatalyst Interfaces: Contrasting Carbon Growth from Ethane and Ethylene. *ACS Applied Nano Materials* 1, 1360–1369.
- LAWRENCE, E. L., LEVIN, B. D. A., BOLAND, T. M., CHANG, S. L. Y. & CROZIER, P. A. (2018). Identification of Rapid Oxygen Exchange Through Site-Dependent Cationic Displacements on CeO2 Nanoparticles. *Microscopy and Microanalysis* 24, 54–55.
- LEVIN, B. D. A., LAWRENCE, E. L. & CROZIER, P. A. (2019). Tracking the Picoscale Motion of Atomic Columns During Dynamic Structural Change. *arXiv:1909.07477 [cond-mat, physics:physics]*. http://arxiv.org/abs/1909.07477 (Accessed September 17, 2019).
- LEVIN, B. D. A., PADGETT, E., CHEN, C.-C., SCOTT, M. C., Xu, R., THEIS, W., JIANG, Y., YANG, Y., OPHUS, C., ZHANG, H., HA, D.-H., WANG, D., Yu, Y., ABRUÑA, H. D., ROBINSON, R. D., ERCIUS, P., KOURKOUTIS, L. F., MIAO, J., MULLER, D. A. & HOVDEN, R. (2016). Nanomaterial datasets to advance tomography in scanning transmission electron microscopy. *Scientific Data* 3, 160041.
- MIGANI, A., NEYMAN, K. M. & BROMLEY, S. T. (2012). Octahedrality versus tetrahedrality in stoichiometric ceria nanoparticles. *Chemical Communications* **48**, 4199.
- MIGANI, A., VAYSSILOV, G. N., BROMLEY, S. T., ILLAS, F. & NEYMAN, K. M. (2010). Dramatic reduction of the oxygen vacancy formation energy in ceria particles: a possible key to their remarkable reactivity at the nanoscale. *Journal of Materials Chemistry* **20**, 10535–10546.
- MÖBUS, G., SAGHI, Z., SAYLE, D. C., BHATTA, U. M., STRINGFELLOW, A. & SAYLE, T. X. T. (2011). Dynamics of Polar Surfaces on Ceria Nanoparticles Observed *In Situ* with Single-Atom Resolution. *Advanced Functional Materials* **21**, 1971–1976.
- MONTINI, T., MELCHIONNA, M., MONAI, M. & FORNASIERO, P. (2016). Fundamentals and Catalytic Applications of CeO₂-Based Materials. *Chemical Reviews* **116**, 5987–6041.
- NILSSON PINGEL, T., JØRGENSEN, M., YANKOVICH, A. B., GRÖNBECK, H. & OLSSON, E. (2018). Influence of atomic site-specific strain on catalytic activity of supported nanoparticles. *Nature Communications* **9**. http://www.nature.com/articles/s41467-018-05055-1 (Accessed August 13, 2018).
- NOLAN, M., FEARON, J. & WATSON, G. (2006). Oxygen vacancy formation and migration in ceria. *Solid State Ionics* **177**, 3069–3074.
- NOOTZ, G. (2012). Fit 2D gaussian function to data. https://www.mathworks.com/matlabcentral/fileexchange/37087-fit-2d-gaussian-function-to-data.

- PAIER, J., PENSCHKE, C. & SAUER, J. (2013). Oxygen Defects and Surface Chemistry of Ceria: Quantum Chemical Studies Compared to Experiment. *Chemical Reviews* **113**, 3949–3985.
- PENG, Z., SOMODI, F., HELVEG, S., KISIELOWSKI, C., SPECHT, P. & BELL, A. T. (2012). High-resolution in situ and ex situ TEM studies on graphene formation and growth on Pt nanoparticles. *Journal of Catalysis* **286**, 22–29.
- SAYLE, T. X. T., PARKER, S. C. & SAYLE, D. C. (2004). Shape of CeO₂ nanoparticles using simulated amorphisation and recrystallisation. *Chemical Communications* 2438.
- SINCLAIR, R., LEE, S. C., SHI, Y. & CHUEH, W. C. (2017). Structure and chemistry of epitaxial ceria thin films on yttria-stabilized zirconia substrates, studied by high resolution electron microscopy. *Ultramicroscopy* **176**, 200–211.
- SKORODUMOVA, N. V., SIMAK, S. I., LUNDQVIST, B. I., ABRIKOSOV, I. A. & JOHANSSON, B. (2002). Quantum Origin of the Oxygen Storage Capability of Ceria. *Physical Review Letters* **89**, 166601.
- STADELMANN, P. (2018). *JEMS, Electron Microscopy Software*. CIME-EPFL: Laussane, Switzerland.
- TAHERI, M. L., STACH, E. A., ARSLAN, I., CROZIER, P. A., KABIUS, B. C., LAGRANGE, T., MINOR, A. M., TAKEDA, S., TANASE, M., WAGNER, J. B. & SHARMA, R. (2016). Current status and future directions for in situ transmission electron microscopy. *Ultramicroscopy* **170**, 86–95.
- TAKEDA, S., KUWAUCHI, Y. & YOSHIDA, H. (2015). Environmental transmission electron microscopy for catalyst materials using a spherical aberration corrector. *Ultramicroscopy* **151**, 178–190.
- TAKEDA, S. & YOSHIDA, H. (2013). Atomic-resolution environmental TEM for quantitative *insitu* microscopy in materials science. *Microscopy* **62**, 193–203.
- TAN, J. P. Y., TAN, H. R., BOOTHROYD, C., FOO, Y. L., HE, C. B. & LIN, M. (2011). Three-Dimensional Structure of CeO₂ Nanocrystals. *The Journal of Physical Chemistry C* 115, 3544–3551.
- TANG, W.-X. & GAO, P.-X. (2016). Nanostructured cerium oxide: preparation, characterization, and application in energy and environmental catalysis. *MRS Communications* **6**, 311–329.
- TAO, F. (FENG) & CROZIER, P. A. (2016). Atomic-Scale Observations of Catalyst Structures under Reaction Conditions and during Catalysis. *Chemical Reviews* **116**, 3487–3539.
- TROVARELLI, A. & LLORCA, J. (2017). Ceria Catalysts at Nanoscale: How Do Crystal Shapes Shape Catalysis? *ACS Catalysis* 7, 4716–4735.

- VENDELBO, S. B., ELKJÆR, C. F., FALSIG, H., PUSPITASARI, I., DONA, P., MELE, L., MORANA, B., NELISSEN, B. J., VAN RIJN, R., CREEMER, J. F., KOOYMAN, P. J. & HELVEG, S. (2014). Visualization of oscillatory behaviour of Pt nanoparticles catalysing CO oxidation. *Nature Materials* 13, 884–890.
- WANG, R., CROZIER, P. A. & SHARMA, R. (2010). Nanoscale compositional and structural evolution in ceria zirconia during cyclic redox treatments. *Journal of Materials Chemistry* **20**, 7497.
- WANG, Z. L. & FENG, X. (2003). Polyhedral Shapes of CeO₂ Nanoparticles. *The Journal of Physical Chemistry B* **107**, 13563–13566.
- YANG, Z., YANG, Y., LIANG, H. & LIU, L. (2009). Hydrothermal synthesis of monodisperse CeO₂ nanocubes. *Materials Letters* **63**, 1774–1777.
- YANG, Z., ZHOU, K., LIU, X., TIAN, Q., LU, D. & YANG, S. (2007). Single-crystalline ceria nanocubes: size-controlled synthesis, characterization and redox property. *Nanotechnology* **18**, 185606.
- YANKOVICH, A. B., BERKELS, B., DAHMEN, W., BINEV, P., SANCHEZ, S. I., BRADLEY, S. A., LI, A., SZLUFARSKA, I. & VOYLES, P. M. (2014). Picometre-precision analysis of scanning transmission electron microscopy images of platinum nanocatalysts. *Nature Communications* 5. http://www.nature.com/articles/ncomms5155 (Accessed August 13, 2018).
- YOSHIDA, H., KUWAUCHI, Y., JINSCHEK, J. R., SUN, K., TANAKA, S., KOHYAMA, M., SHIMADA, S., HARUTA, M. & TAKEDA, S. (2012). Visualizing Gas Molecules Interacting with Supported Nanoparticulate Catalysts at Reaction Conditions. *Science* **335**, 317–319.